Intraoperative Evaluation of Breast Tumor Margins with Optical Coherence Tomography

Freddy T. Nguyen,[1,3,4] Adam M. Zysk,[2,4] Eric J. Chaney,[4] Jan G. Kotynek,[5,7] Uretz J. Oliphant,[5,7] Frank J. Bellafiore,[5,7] Kendrith M. Rowland,[5,7] Patricia A. Johnson,[5,7] and Stephen A. Boppart[2,3,4,5,6,7]

Departments of [1]Chemistry and [2]Electrical and Computer Engineering, [3]College of Medicine, and [4]Beckman Institute for Advanced Science & Technology, University of Illinois at Urbana-Champaign; [5]Mills Breast Cancer Institute, [6]Carle Foundation Hospital, and [7]Carle Clinic Association, Urbana, Illinois

Abstract

As breast cancer screening rates increase, smaller and more numerous lesions are being identified earlier, leading to more breast-conserving surgical procedures. Achieving a clean surgical margin represents a technical challenge with important clinical implications. Optical coherence tomography (OCT) is introduced as an intraoperative high-resolution imaging technique that assesses surgical breast tumor margins by providing real-time microscopic images up to 2 mm beneath the tissue surface. In a study of 37 patients split between training and study groups, OCT images covering 1 cm^2 regions were acquired from surgical margins of lumpectomy specimens, registered with ink, and correlated with corresponding histologic sections. A 17-patient training set used to establish standard imaging protocols and OCT evaluation criteria showed that areas of higher scattering tissue with a heterogeneous pattern were indicative of tumor cells and tumor tissue in contrast to lower scattering adipocytes found in normal breast tissue. The remaining 20 patients were enrolled into the feasibility study. Of these lumpectomy specimens, 11 were identified with a positive or close surgical margin and 9 were identified with a negative margin under OCT. Based on histologic findings, 9 true positives, 9 true negatives, 2 false positives, and 0 false negatives were found, yielding a sensitivity of 100% and specificity of 82%. These results show the potential of OCT as a real-time method for intraoperative margin assessment in breast-conserving surgeries. [Cancer Res 2009;69(22):8790–6]

Introduction

Breast cancer. Improved breast cancer screening has resulted in smaller lesions being detected earlier. An estimated 192,370 new cases of invasive breast cancer (26% of newly diagnosed cancer cases in women), 62,280 new cases of ductal carcinoma *in situ*, and 40,610 breast cancer deaths will be reported in the United States during 2009, making it the most widely diagnosed cancer and the second leading cause of cancer deaths among women (1). Increased 5-year survival rates have been attributed to increased awareness, earlier detection, and improved treatment and management. A large portion of patients undergo surgical removal of lesions via breast-conserving surgery (lumpectomy) with irradiation often accompanied by sentinel or axillary lymph node dissection for disease staging.

Tumor margin assessment and local recurrence. As lumpectomy rates have increased over time, the definition of a clean margin has changed. A recent study reported 45.9% of radiation oncologists defined negative margins as no cancer cells at inked margins, whereas 7.4% defined it as no cells within 1 mm and 21.8% believed it to be no cells within 2 mm (2). As more studies correlated the width of uninvolved margins to local recurrence (3, 4), a more aggressive approach toward breast conservation has allowed surgeons to use 2 mm, or even 1 mm, to define a clean margin. The same survey of radiation oncologists reported that 31% of respondents defined a close margin as having no cells within 1 mm and an additional 38% defined it to be no cells within 2 mm of the inked surface (2).

Despite this ongoing debate, the key predictor of local recurrence is the margin status (5–16). A positive margin, the presence of disease on the inked surface, occurs in at least 30% to 35% of cases, and an additional 10% to 15% are classified as close margins (<2 mm; ref. 15). Local recurrence rates for breast-conserving therapy followed by radiation were reported in 2% to 28% of cases with positive margins, 2% to 16% with close margins (<2 mm), and 2% to 8% with negative margins (15), which would be higher in the absence of radiation therapy (6, 8, 17, 18).

Intraoperative margin assessment. Currently, no real-time, nondestructive intraoperative method exists to rapidly assess the microscopic status of lumpectomy margins as standard of care (19, 20). Several techniques have been investigated including frozen section analysis, touch prep cytology, radiography, radiofrequency spectroscopy, and Raman spectroscopy. Frozen section analysis was reported to have a sensitivity of 73.08% and a specificity of 98.32% compared with paraffin section analysis in breast cancer (19). Frozen section analysis has not widely been accepted as part of standard of care due to difficulties in performing frozen sections on adipose tissue, added time (~20-30 min), increased operating room time, and additional pathology evaluation with increased costs. The most significant disadvantage is the inability for frozen section analysis to be done over the entire surface area of the tissue specimen, sharing the same sampling rate limitation as paraffin section analysis in sampling only 10% to 15% of the surface area (21).

Touch prep cytology can rapidly assess the entire surface area, addressing the sampling rate issue, while preserving the integrity of the specimen, and making it a promising technique for identifying positive margins. This technique reported a sensitivity of 75% and a specificity of 82.8% (21). The major disadvantages include the requirement for tumor cells to be at the surface, and

Requests for reprints: Stephen A. Boppart, University of Illinois at Urbana-Champaign, 405 North Mathews Avenue, Urbana, IL 61801. Phone: 217-244-7479; Fax: 217-333-5833; E-mail: boppart@illinois.edu.

doi:10.1158/0008-5472.CAN-08-4340

their detachment. Touch prep cytology does not provide information about the presence of cancer cells beneath the surface and therefore is unable to determine close and negative margins.

Intraoperative radiography of specimens provides surgeons the ability to visualize the margin in-depth by displaying two-dimensional X-ray projections. However, the low reported sensitivity and specificity of 49% and 73%, respectively (22), are primarily due to the inability to identify diffuse microscopic processes, especially where the tumor boundary is poorly defined (23).

Radiofrequency spectroscopy provides a bulk measurement over a circular area (diameter = 0.7 cm) and within a 100 μm depth (24). With low sensitivity (71%) and specificity (68%; ref. 24), shallow penetration depth, and low resolution, detection within 1 to 2 mm for margin classification is limited.

Raman spectroscopy, which extracts chemical information, was reported to have a sensitivity of 100%, a specificity of 100%, and overall accuracy of 93% in identifying carcinomas (25). Despite high sensitivity and specificity, this technique may have limited clinical utility due to point measurements with long 1 s acquisition times per point, making it unable to quickly sample large surface areas with high spatial resolution.

Optical coherence tomography in breast cancer. Optical coherence tomography (OCT) is a high-resolution microscopic optical imaging technique that yields real-time multidimensional images of subsurface tissue structure (26–32). OCT is the optical analogue to ultrasound imaging but uses light waves instead of sound waves to create images. Near-infrared light enables micron-scale resolution, providing images on the same resolution scale as histopathology. The penetration depth in breast tissue is ~1 to 2 mm, making OCT a suitable technology for intraoperative tumor margin assessment. The density of cells and subcellular scatterers (nuclei and organelles) primarily determines the depth to which the OCT light penetrates tissue and scatters back to be detected. Tissue composed primarily of adipocytes can be imaged to depths of 2 mm compared with 200 to 1,000 μm in cell-dense tumor tissue. These depths are comparable with the currently accepted margin widths that classify positive, close, and negative margins. By enabling surgeons to rapidly visualize tissue morphology beneath the surface and over large surface areas while preserving tissue structure, OCT has the potential to become an invaluable intraoperative tool for assessing margin status.

Since its introduction, OCT has capitalized on advances in telecommunications, resulting in significant increases in data acquisition speeds (33), added functional modalities (34–36), and new contrast agents (37, 38). OCT has found clinical applications in ophthalmology, cardiology, gastroenterology, and oncology (39). OCT has been used to image tumor margins in a *N*-methyl-*N*-nitrosourea carcinogen-induced rat mammary tumor model, differentiating between highly scattering cancer cells and the fibrous/fatty tissue associated with normal mammary tissue (29, 40). Increased scattering in tumor is attributed to the increase in nuclear-to-cytoplasm ratio and the increase in cellular and nuclear density (41, 42). The large size and low scattering of adipocytes, relative to higher scattering stromal and tumor cells, provides one method for differentiating these tissue types (29, 40, 43).

Access to deep breast lesions can be done using needle-based OCT probes (43–45). These needle probes can provide real-time information for guided lesion biopsy or for placement of localization wires (44, 45). Reports identified diagnostically significant information within the optical backscattering and refractive index signals that can distinguish various breast tissue types (29, 40, 46). These same diagnostic properties can be extracted from individual axial scans that comprise an OCT image or from spatial information provided by the OCT image itself (40, 45, 46). This study focuses on the first intraoperative OCT assessment of exposed tumor margins.

Materials and Methods

Instrument. A clinical spectral-domain OCT system (Figs. 1 and 2) was constructed to assess surgical margins from lumpectomy specimens. The OCT system employs a superluminescent diode (model SLD1C; B&W Tek), with an optical spectrum centered at 1,310 nm and a bandwidth of 92 nm. Light is passed through an optical circulator (CIRC-3-31-P-BB-10-6:3port; Gould Fiber Optics) and into a 95/5 fiber-optic splitter (Gould Fiber Optics) that divides the light into a sample and reference arm. A 60 mm focal length achromatic lens in the sample arm focuses 4.75 mW light to a 35 μm spot (transverse resolution). The broad bandwidth source yields an axial resolution of 5.9 μm in tissue. The depth of field of the lens (1.47 mm) closely matches the penetration depth of OCT in human breast tissue. Reflected light from the sample and reference arms is passed through polarization controllers (FPC-2; Fiber Control), coupled into an interferometer, spectrally dispersed by a diffraction grating (53004BK01-148R; Richardson Gratings, Newport; 1,000 grooves/mm and blazed for 1,310 nm), and focused onto an indium gallium arsenide line camera (SU1024LE-1.7T1-0500; Sensors Unlimited) with a 150 mm singlet lens. With camera exposure times ranging from 24.4 to 408.4 μs, corresponding measured signal-to-noise ratios ranged from 96 to 116 dB. The imaging system acquires OCT images at a rate of ~5,000 axial scans/s or up to ~8 to 9 images/s (~600 axial scans/10 mm). The sample is laterally scanned under the OCT beam using an automated translation stage. Data are collected using a high-speed data acquisition card with a 5 MHz sampling rate and 12-bit quantizer

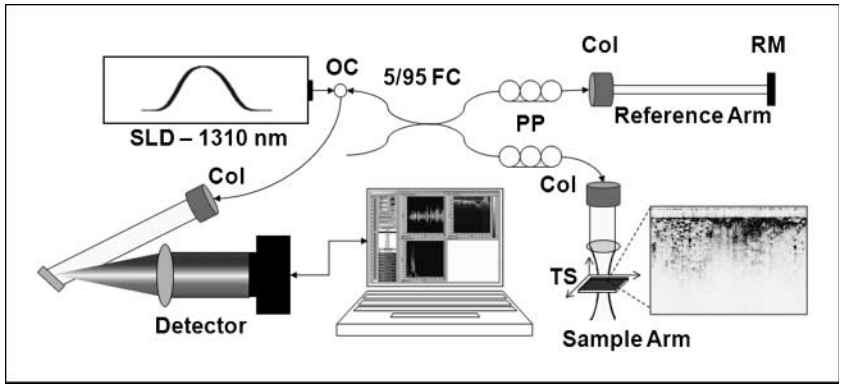

Figure 1. Clinical spectral-domain OCT system schematic. Light from a superluminescent diode (λ = 1,310 nm) is directed into an optical circulator (*OC*) and to a fiber coupler (*FC*), which splits 5% of the light to a reference arm mirror (*RM*) and 95% of the light to a sample arm containing focusing optics and an automated *x-y* translation stage (*TS*). Light is collimated through fiber collimators (*Col*). Reflected light from each arm is coupled through polarization paddles (*PP*), interfered within the fiber coupler, and spectrally dispersed onto a line camera.

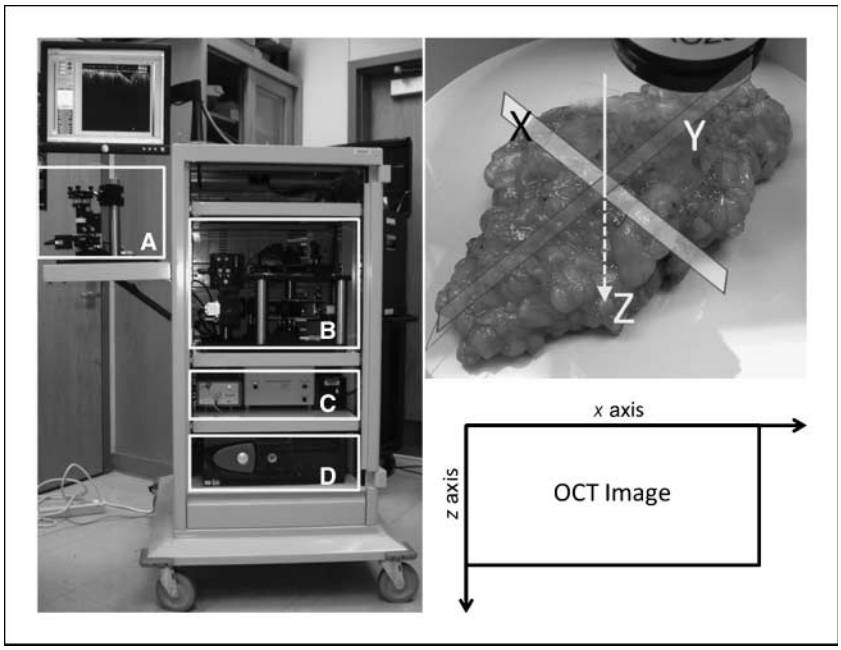

Figure 2. Photograph of the clinical spectral-domain OCT system housed in a standard endoscopy cart (*left*). This system is portable for use in various surgical suites. Resected surgical specimens are placed on the sample-arm stage (*A*). The detector and reference arm (*B*) are located within the cart along with the light source and hardware controllers (*C*) and computer (*D*). OCT images (shown in later figures) represent two-dimensional cross-sectional planes (*x-z*) oriented perpendicular to the tissue surface (*right*). Multiple OCT images can be acquired by stepping the beam in the *y* direction.

(PCI-6111E; National Instruments) in a dual Xeon processor (3.20 GHz) computer with 1 GB of RAM. Acquisition and processing time for an OCT image was ~5 s/image. The OCT hardware and data acquisition are controlled by custom software written in LabView and interfaced with a data processing sequence written in Matlab/C++. Due to the nonlinear response from optical components, a cubic spline interpolation and resampling technique is implemented to compensate for aberrations (47). The data are assembled and displayed as two-dimensional images.

Imaging protocol. Patients identified and recruited for this study had primary breast tumors (both *in situ* and invasive carcinoma) in need of surgical resection by breast-conserving surgery, as determined by physicians at Carle Foundation Hospital and Carle Clinic Association, based on preoperative radiologic films, biopsy results, or other relevant diagnostic information. Patients undergoing mastectomy were excluded due to decreased likelihood of positive or close margins. No patients were excluded due to age or race. Patients were consented before surgery per protocols approved by institutional review boards at the University of Illinois at Urbana-Champaign and Carle Foundation Hospital. After surgical tissue resection but before margin assessment by the radiologist or pathologist, initial lumpectomy specimens were imaged in the operating room using OCT (Fig. 2). A series of 10 to 20 parallel images were taken over a 1.0 × 1.0 cm area. The researchers involved in image acquisition varied between imaging sessions and no information about the specimen was disclosed by the surgeon or staff during the sessions. Regions selected for OCT were based on suspicious visual or palpable findings as determined by the researchers or were the entry-exit sites of localization guide wires. Following OCT imaging, one imaging site per specimen was marked with ink for correlation with histopathology, and the specimen was returned to surgical staff for standard processing and pathologic margin assessment. In addition to histology sections acquired for diagnostic purposes as part of standard of care, sections coregistered with intraoperative OCT were acquired, stained, and correlated.

OCT image processing and evaluation protocol. All OCT images were processed with the same standardization method and displayed on the same intensity scale (47). OCT images were initially evaluated in real-time by one of several researchers trained on the characteristic features found on OCT of breast tissue to ensure that the images were of sufficient quality for evaluation and to ensure that a subset of the images collected contained diagnostic features. Using criteria established from the training set, a single researcher during a single session, several months after data sets were acquired, evaluated all OCT images, identifying normal or abnormal features. Images with abnormal features were classified as positive because the OCT imaging depth was within the 2 mm range commonly used to define close margins and because the OCT image features were thought to be indicative of invasive or *in situ* carcinoma. Because 10 to 20 OCT images were taken at each imaging site and correlated to a single histologic section from that site, OCT margin assessment was made using the full set of available OCT images for each site.

Histology image evaluation protocol. Histology sections were acquired from marked areas imaged in the operating room with OCT. All tissue sections were stained with H&E and some were additionally immunohistochemically stained. Histology slides were digitized using a light microscope at 4× magnification and stitched together (Adobe Photoshop) to produce a single image. The compiled montage was oriented based on inked borders for later correlation to OCT images. H&E-stained histology images were classified by a board-certified pathologist as invasive carcinoma, *in situ* carcinoma, other abnormal tissue, or normal tissue. Margins identified as carcinoma or other abnormal tissues were considered to be positive. The pathologist was blinded to the OCT images and results, giving an independent and unbiased assessment of the histology slide corresponding to the matching OCT image set.

Results

Patient demographics. A total of 37 female patients were enrolled in the study. The training set consisted of 17 patients with a mean age of 62 years (range, 44-82) and the study set consisted of 20 patients with a mean age of 66 years (range, 41-84). Their final diagnoses, based on pathologic findings and tumor margin assessments, included 15 cases of ductal carcinoma *in situ*, 1 case of lobular carcinoma *in situ*, 2 cases of infiltrating ductal carcinoma, 9 cases of invasive ductal carcinoma, 1 case of invasive papillary carcinoma, 2 cases of invasive mammary carcinoma, and 1 case of atypical ductal hyperplasia. The majority had more than one diagnosis classification associated with their histopathologic assessment. An additional 2 patients in the training set and 2 patients in the study set were consented but subsequently excluded from the study and OCT imaging due to changes in surgery schedules or procedures.

Training data set. An initial training data set of 78 OCT images from 17 patients (minimum = 2, maximum = 10, average = 5

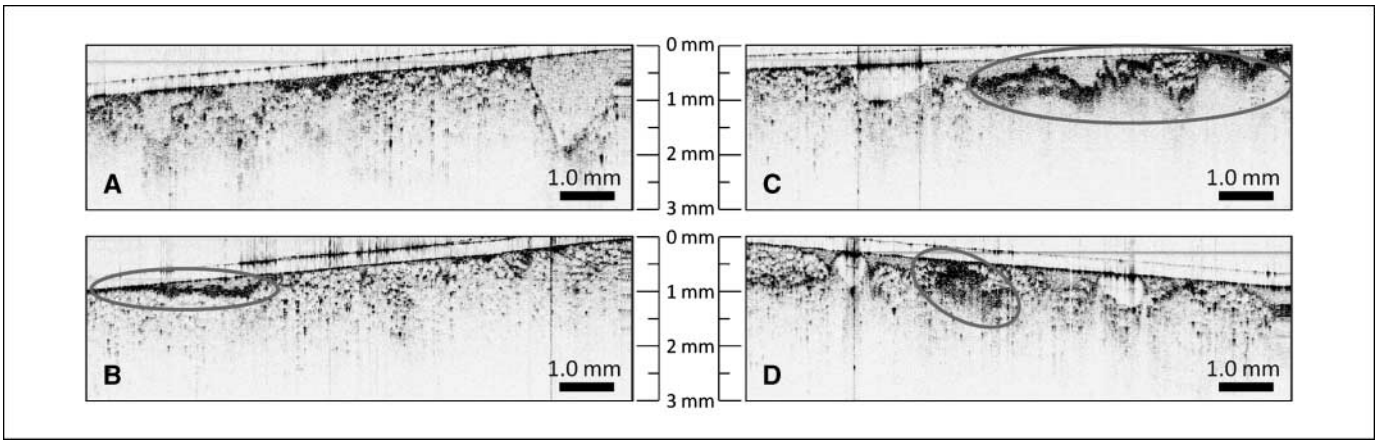

Figure 3. Representative OCT images of surgical margins from lumpectomy specimens acquired for the training set. Images of normal tissue (*A*) were identified by the homogenous pattern of large adipose cells. Readily identified surgical artifacts include blood (*B*), which appears as a thin film of scatterers, and cauterized tissue (*C*), which has a patch-like appearance. Images of positive margins (*D*) containing tumor cells and tissue included a highly scattering area that was more heterogeneous and disruptive of the surrounding architecture.

images/specimen) were used to establish standard imaging protocols, coregistration procedures, and image evaluation criteria of the surgical margins. Representative images shown in Fig. 3 include normal adipose tissue (Fig. 3*A*), surgical artifacts of surface blood (Fig. 3*B*) and cauterized tissue (Fig. 3*C*), areas that appear duct-like in shape (Fig. 3*D*), and areas of highly scattering cells with spatially heterogeneous scattering intensity (Fig. 3*D*). These results were confirmed by gross visual findings or by histopathologic analysis. Histopathologic analysis reported ductal carcinoma *in situ* involvement for the specimen imaged in Fig. 3*D*. The training data set findings were used to establish the evaluation methodology and image feature criteria for identifying positive margins. These criteria included the presence or absence of high-intensity scatterers, the location of these scatterers throughout the tissue, the heterogeneous/homogeneous spatial distribution of scattering intensity, and the morphologic characteristics of these regions of interest. Surgical artifacts that could interfere with OCT evaluation such as surface blood and cauterized tissue appear as contiguous and highly scattering areas, remain localized to the immediate surface, and were quickly identified visually in the imaging field. In Fig. 3*B*, a thin film (<100 μm) of homogeneous scatterers is representative of a bloody surface, whereas, in Fig. 3*C*, the cauterized tissue produced a highly scattering area, which was observed within ~300 μm of the tissue surface. The region of interest in Fig. 3*D* has both a high scattering intensity and a more heterogeneous composition indicative of cancerous tissue. In Fig. 3*D*, the presence of highly scattering regions deep in the margin, instead of localized to the immediate surface, increases the likelihood that these features are intrinsic to the tissue architecture rather than a result of the surgical procedure.

Study data set. OCT images with histologic correlations from an additional 20 patients were used for the study set. A total of 210 OCT images were acquired from 20 lumpectomy specimens with an average of 10 OCT images per specimen. Using criteria established from the training set, the study set was evaluated and specimen margins were classified as positive or negative. A margin was considered positive if there was evidence of tumor cells or tissue either at the immediate surface or within the imaging depth of OCT (1-2 mm). Eleven margins were identified as positive and 9 as negative under OCT image analysis. Analysis of corresponding H&E-stained histologic sections yielded 9 true positives, 9 true negatives, 2 false positives, and 0 false negatives, giving a sensitivity of 100% and specificity of 82% (Table 1). Overall accuracy of OCT was 90% with a positive predictive value and a negative predictive value of 82% and 100%, respectively.

Three representative cases from the study set are presented in Figs. 4 and 5. The first patient (female, age 66 years) was diagnosed with ductal carcinoma *in situ* via ultrasound-guided core-needle biopsy with a 3.0 cm primary tumor. This case (Fig. 4) shows OCT assessment of a negative tumor margin, which consists primarily of large lipid-filled adipocytes with interweaving microvasculature. The small dark highly scattering point-like regions in the OCT image correspond to individual nuclei of adipocytes. Histologic evaluation indicated that tumor cells were located >3 mm from the surface, confirming the OCT findings of a negative margin.

A second patient (female, age 60 years), diagnosed with invasive papillary carcinoma via ultrasound-guided core-needle biopsy, had a 0.8 cm primary tumor removed by lumpectomy. A third patient (female, age 51 years) was diagnosed with poorly differentiated infiltrating ductal carcinoma and high-grade ductal carcinoma *in situ*

Table 1. Intraoperative tumor margin assessment (OCT versus histopathology)

	Histology (positive)	Histology (negative)	Total	
OCT (positive)	9 (true positive)	2 (false positive)	11	Positive predictive value = 82%
OCT (negative)	0 (false negative)	9 (true negative)	9	Negative predictive value = 100%
Total	9	11	20	
	Sensitivity = 100%	Specificity = 82%		

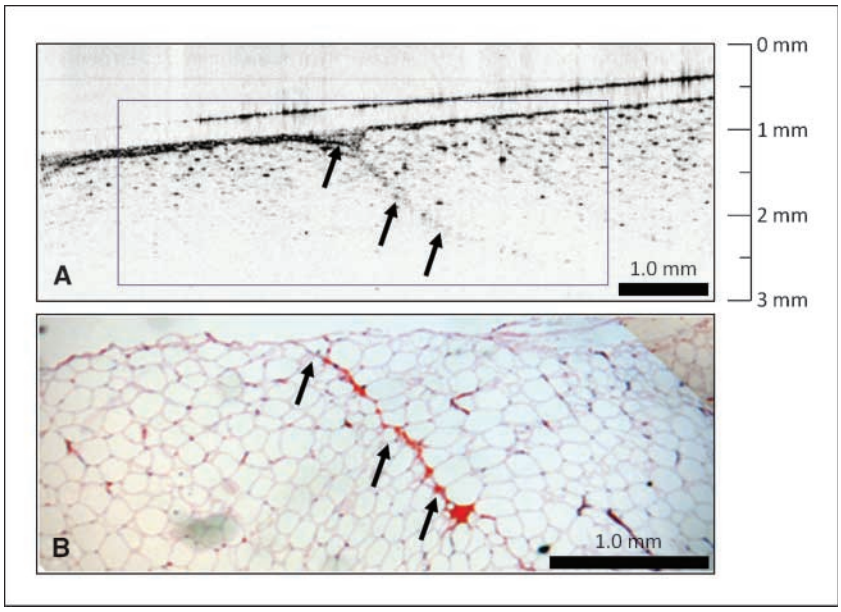

Figure 4. Negative tumor margin. OCT (*A*) and corresponding H&E-stained histology (*B*) of normal breast tissue near the surface of a lumpectomy specimen. The large adipose cells with point-like scattering nuclei dominate the OCT image, which also contains a region of the microvasculature (*arrows*). Features found in the real-time intraoperative OCT image correspond well to those identified in the postsurgical paraffin-embedded histology section.

with a 2.3 cm primary tumor. Intraoperative OCT imaging of the margins (Fig. 5) revealed suspicious regions with increased and heterogeneous scattering within 1 mm of the inked surface (Fig. 5*A*, patient 2, 60 F) and within 0.5 to 1.25 mm of the surface (Fig. 5*C*, patient 3, 51 F). The matching H&E-stained histology sections for the OCT images shown in Fig. 5*A* and *C* are provided in Fig. 5*B* and *D*, respectively, confirming the diagnostic features observed. These areas contained small and highly scattering cells contributing to the increased contrast when compared with adjacent adipocytes. The increased scattering is from strong reflections from tightly packed cells, which provides the contrast observed in OCT. These results show distinct structural features identified with real-time intraoperative OCT on unstained tissue specimens that can be used to identify positive and negative margins without compromising the structural integrity of the specimens.

Discussion

This study presents the first intraoperative demonstration of OCT as a real-time, high-resolution imaging technique for the microscopic assessment of breast tumor margins. By providing subsurface imaging capabilities 1 to 2 mm deep with micron-scale resolution, OCT provides surgeons the ability to assess margin status in real-time, complementing current gross visual examination, potentially reducing the number of positive/close margins discovered postoperatively, and thereby reducing the need for additional surgical procedures. In the current standard-of-care, pathologists perform microscopic margin assessment within the 2 mm range of the surface using frozen section analysis or paraffin section analysis to determine the need for additional tissue removal.

OCT identified areas of homogeneous adipocytes, suspicious regions with highly scattering and tightly packed cells, and heterogeneous scattering patterns as some of the key features used to classify margins as negative or positive as verified by histopathology. The large relative cell size difference easily separates the identification of adipocytes from tumor cells and stromal tissue. Increased nuclear density and changes in chromatin texture are believed to be responsible for high levels of scattering observed from cancer cells (41, 42). At later tumor stages, observed characteristics change from open to filled ducts and lobules and to heterogeneous tumor masses. Focal

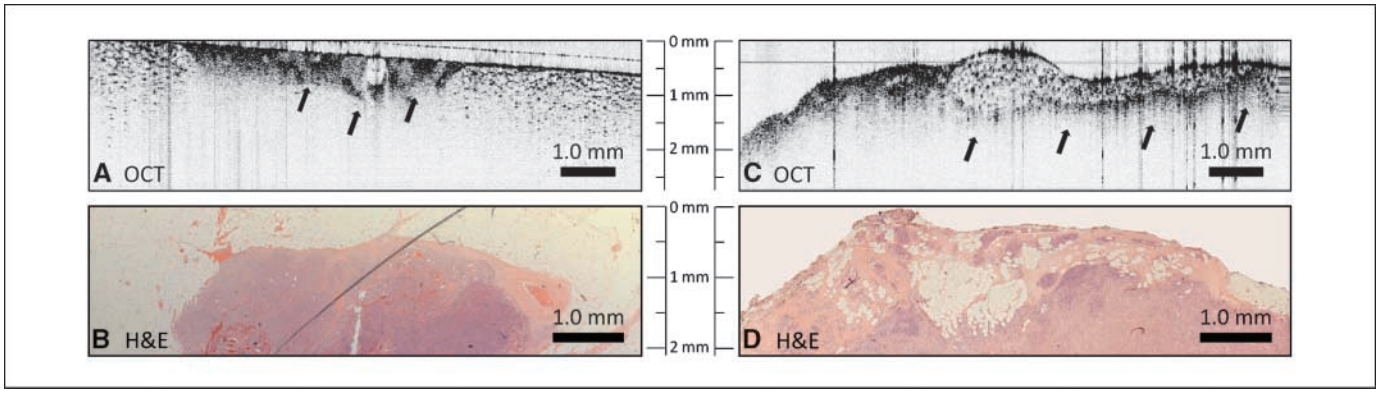

Figure 5. Positive tumor margins. OCT images (*A* and *C*) show a distinct heterogeneously scattering region (*arrows*) with small, highly scattering foci indicative of collections of tumor cells. These features clearly extend to the surface of the specimen (to the surgical margin) in *A* and the left side of *C* but also are evident below adipose tissue in *C*. The OCT image in *A* was acquired with a coverslip over the surface to reduce back-reflection artifacts, which appear as vertical lines in *C*. Corresponding H&E-stained histology (*B* and *D*) images show corresponding features, confirming the presence of these positive margins.

regions of scatterers embedded in adipose tissue were identified under OCT indicative of smaller clusters of tumor cells. With more advanced cancer, areas of highly scattering tissue with irregular and heterogeneous patterns were identified. With an increased sampling rate of tumor margins with OCT, we expect to identify an increased number of positive surgical margins not otherwise grossly identifiable and likely missed due to limited sampling during standard histopathologic analysis.

Surgical artifacts such as cauterized tissue and superficial blood are identified in OCT images as a contiguous layer of dark scatterers. These artifacts appear homogeneous in nature and are limited to the cut surface of the surgical margin rather than extending deep into the tissue. A relatively large pool of blood or cauterized tissue can limit the penetration depth of OCT due to high scattering. The imaging penetration depth with a bloody surface (Fig. 3*B*) is slightly diminished, compared with a cauterized surface (Fig. 3*C*), where penetration depth drops off sharply with little to no features observed beyond the cauterized tissue. Intravascular blood in small vessels and capillaries makes up a relatively small percentage of the tissue volume and has a minimal effect on the OCT penetration depth. In cases with residual surface blood, saline has been used to rapidly irrigate the surface to regain OCT imaging depth. OCT has been shown for *in vivo* intravascular applications in humans, where an OCT imaging catheter is fully immersed in blood and imaging is done following a saline flush (48). These surgical artifacts can be differentiated from intrinsic tissue properties and can be quickly addressed without interfering with the ability of OCT to assess the margin. The presence of dyes such as methylene blue or lymphazurin, which are used to map lymph drainage for sentinel and axillary lymph node dissections, absorb in the spectral region below 700 nm (data not shown). Therefore, the presence of these dyes does not affect OCT imaging because our system operates in the spectral region around 1300 nm.

Recent advances in OCT technology have increased data acquisition speeds to ≥200,000 axial scans/s (33). This would permit acquisition of 400 frames/s for a scan range of 10 mm and a lateral resolution of 35 μm. For a 1 cm^2 area, imaging would be achieved in a few seconds while maintaining the full lateral resolution in both *x* and *y* directions. Novel computational algorithms such as interferometric synthetic aperture microscopy are being implemented for real-time OCT imaging, yielding spatially invariant lateral resolution equivalent to that achieved at the focus of the beam (49). These combined advances offer the potential to vastly increase data acquisition rates and resolution without sacrificing the large scan area and real-time capabilities of OCT. The significant increase in data volume and limited time to analyze and interpret image sets will increase the need for automated classification algorithms (40, 44).

The differentiation of malignant (carcinoma) from benign (fibroadenoma) tumors is an ongoing research effort, as with many other biomedical imaging techniques. Stromal tissue, which makes up a larger percentage of breast tissue in younger patients, is primarily composed of connective tissue and favorably is generally less scattering compared with tumor tissue (50). Studies have shown that the optical refractive index does not differ greatly between stromal and tumor tissue (46). Preliminary results from our laboratory have identified a promising combined method for distinguishing between the two tissue types by examining the power attenuation in the signal, the periodicity of the scattering profile, and the extracted refractive index information to aid in automated classification of OCT signals (40, 45, 46). Differentiation between benign fibrocystic changes versus malignant lesions will be important in further clinical studies. Cysts are expected to be readily distinguished due to their relatively large size, thin membranes, and low amount of scatterers within the cyst. Early morphologic changes such as ductal hyperplasia or dysplasia, with increased cell density and nuclear-to-cytoplasm ratio, are likely to exhibit increased scattering, and ongoing work to improve resolution and to extract distinct image features may be necessary to distinguish these early changes.

This report shows the potential of real-time intraoperative OCT for margin assessment from resected breast lumpectomy specimens. OCT acquires images in the same physical range as that used in histology to classify surgical margins as positive, close (<2 mm), or negative. The development of faster scanning handheld probes will allow surgeons to quickly scan the *in situ* tumor cavity wall in addition to the lumpectomy specimen margin, providing guidance on tissue removal. *In situ* OCT imaging would effectively double the sampling depth by evaluating depths up to 2 mm on the specimen and on the cavity wall. Further studies with even higher resolution, comprehensive volumetric imaging, and automated tissue-type classification are expected to reveal additional unique features that can be used to further improve the identification of positive and negative margins intraoperatively with OCT. Intraoperative identification of positive margins will decrease the need for additional surgical procedures and the rate of local recurrence in breast cancer patients.

Disclosure of Potential Conflicts of Interest

S.A. Boppart is cofounder of Diagnostic Photonics, Inc., a company developing Interferometric Synthetic Aperture Microscopy for intraoperative imaging. He also receives royalties from patents related to optical coherence tomography, licensed from the Massachusetts Institute of Technology. The other authors disclosed no potential conflicts of interest.

Acknowledgments

Received 11/30/08; revised 9/11/09; accepted 9/16/09; published online 11/12/09.

Grant support: NIH grant R01 EB005221, University of Illinois at Urbana-Champaign and University of Illinois at Chicago Intercampus Research Initiative in Biotechnology, Grainger Foundation, and Carle Foundation Hospital (S.A. Boppart) and U.S. Department of Defense grant BC073292 (F.T. Nguyen).

Additional information can be found at http://biophotonics.illinois.edu.

The costs of publication of this article were defrayed in part by the payment of page charges. This article must therefore be hereby marked *advertisement* in accordance with 18 U.S.C. Section 1734 solely to indicate this fact.

We thank Ann Benefiel, Mary Collins, Barbara Hall, and the research support staff and administration at Carle Foundation Hospital and Carle Clinic Association for their assistance in coordinating the clinical aspects of this study. We also thank Dr. Daniel L. Marks for technical discussions and contributions toward this project.

References

1. Cancer facts & figures 2009. Atlanta: American Cancer Society; 2009.
2. Taghian A, Mohiuddin M, Jagsi R, Goldberg S, Ceilley E, Powell S. Current perceptions regarding surgical margin status after breast-conserving therapy: results of a survey. Ann Surg 2005;241:629–39.
3. Dillon MF, Hill AD, Quinn CM, McDermott EW, O'Higgins N. A pathologic assessment of adequate margin status in breast-conserving therapy. Ann Surg Oncol 2006;13:333–9.
4. Luini A, Rososchansky J, Gatti G, et al. The surgical margin status after breast-conserving surgery: discussion of an open issue. Breast Cancer Res Treat 2008; 113:397–402.
5. Aziz D, Rawlinson E, Narod SA, et al. The role of reexcision for positive margins in optimizing local disease

control after breast-conserving surgery for cancer. Breast J 2006;12:331–7.

6. Cefaro GA, Genovesi D, Marchese R, et al. Predictors of local recurrence after conservative surgery and whole-breast irradiation. Breast Cancer Res Treat 2006;98:329–35.

7. Cellini C, Hollenbeck ST, Christos P, et al. Factors associated with residual breast cancer after re-excision for close or positive margins. Ann Surg Oncol 2004;11: 915–20.

8. Connolly JL, Boyages J, Nixon AJ, et al. Predictors of breast recurrence after conservative surgery and radiation therapy for invasive breast cancer. Mod Pathol 1998;11:134–9.

9. Dillon MF, Mc Dermott EW, O'Doherty A, Quinn CM, Hill AD, O'Higgins N. Factors affecting successful breast conservation for ductal carcinoma *in situ*. Ann Surg Oncol 2007;14:1618–28.

10. Huston TL, Pigalarga R, Osborne MP, Tousimis E. The influence of additional surgical margins on the total specimen volume excised and the reoperative rate after breast-conserving surgery. Am J Surg 2006;192:509–12.

11. McIntosh A, Freedman G, Eisenberg D, Anderson P. Recurrence rates and analysis of close or positive margins in patients treated without re-excision before radiation for breast cancer. Am J Clin Oncol 2007;30:146–51.

12. Schouten van der Velden AP, Van de Vrande SL, Boetes C, Bult P, Wobbes T. Residual disease after re-excision for tumour-positive surgical margins in both ductal carcinoma *in situ* and invasive carcinoma of the breast: the effect of time. J Surg Oncol 2007;96: 569–74.

13. Scopa CD, Aroukatos P, Tsamandas AC, Aletra C. Evaluation of margin status in lumpectomy specimens and residual breast carcinoma. Breast J 2006;12:150–3.

14. Smitt MC, Nowels KW, Zdeblick MJ, et al. The importance of the lumpectomy surgical margin status in long-term results of breast conservation. Cancer 1995; 76:259–67.

15. Swanson GP, Rynearson K, Symmonds R. Significance of margins of excision on breast cancer recurrence. Am J Clin Oncol 2002;25:438–41.

16. Zavagno G, Goldin E, Mencarelli R, et al. Role of resection margins in patients treated with breast conservation surgery. Cancer 2008;112:1923–31.

17. Cefaro GA, Genovesi D, Marchese R, et al. The effect of delaying adjuvant radiation treatment after conservative surgery for early breast cancer. Breast J 2007;13: 575–80.

18. van der Velden AP, Peeters PH, Koot VC, Hennipman A. Local recurrences after conservative treatment of ductal carcinoma-*in-situ* of the breast without radiotherapy: the effect of age. Ann Surg Oncol 2006;13:990–8.

19. Olson TP, Harter J, Munoz A, Mahvi DM, Breslin T. Frozen section analysis for intraoperative margin assessment during breast-conserving surgery results in low rates of re-excision and local recurrence. Ann Surg Oncol 2007;14:2953–60.

20. McLaughlin SA, Ochoa-Frongia LM, Patil SM, Cody HS III, Sclafani LM. Influence of frozen-section analysis of sentinel lymph node and lumpectomy margin status on reoperation rates in patients undergoing breast-conservation therapy. J Am Coll Surg 2008;206: 76–82.

21. Valdes EK, Boolbol SK, Cohen JM, Feldman SM. Intra-operative touch preparation cytology; does it have a role in re-excision lumpectomy? Ann Surg Oncol 2007; 14:1045–50.

22. Goldfeder S, Davis D, Cullinan J. Breast specimen radiography: can it predict margin status of excised breast carcinoma? Acad Radiol 2006;13:1453–9.

23. Erguvan-Dogan B, Whitman GJ, Nguyen VA, et al. Specimen radiography in confirmation of MRI-guided needle localization and surgical excision of breast lesions. AJR Am J Roentgenol 2006;187:339–44.

24. Karni T, Pappo I, Sandbank J, et al. A device for real-time, intraoperative margin assessment in breast-conservation surgery. Am J Surg 2007;194:467–73.

25. Haka AS, Volynskaya Z, Gardecki JA, et al. *In vivo* margin assessment during partial mastectomy breast surgery using Raman spectroscopy. Cancer Res 2006; 66:3317–22.

26. Boppart SA, Bouma BE, Pitris C, Southern JF, Brezinski ME, Fujimoto JG. *In vivo* cellular optical coherence tomography imaging. Nat Med 1998;4:861–5.

27. Boppart SA, Bouma BE, Pitris C, et al. Intraoperative assessment of microsurgery with three-dimensional optical coherence tomography. Radiology 1998;208:81–6.

28. Boppart SA, Deutsch TF, Rattner DW. Optical imaging technology in minimally invasive surgery. Current status and future directions. Surg Endosc 1999; 13:718–22.

29. Boppart SA, Luo W, Marks DL, Singletary KW. Optical coherence tomography: feasibility for basic research and image-guided surgery of breast cancer. Breast Cancer Res Treat 2004;84:85–97.

30. Bouma BE, Tearney GJ. Handbook of optical coherence tomography. New York: Marcel Dekker; 2002.

31. Fujimoto JG, Pitris C, Boppart SA, Brezinski ME. Optical coherence tomography: an emerging technology for biomedical imaging and optical biopsy. Neoplasia 2000;2:9–25.

32. Huang D, Swanson EA, Lin CP, et al. Optical coherence tomography. Science 1991;254:1178–81.

33. Huber R, Adler DC, Fujimoto JG. Buffered Fourier domain mode locking: unidirectional swept laser sources for optical coherence tomography imaging at 370,000 lines/s. Opt Lett 2006;31:2975–7.

34. de Boer JF, Milner TE, van Gemert MJ, Nelson JS. Two-dimensional birefringence imaging in biological tissue by polarization-sensitive optical coherence tomography. Opt Lett 1997;22:934–6.

35. Oldenburg AL, Crecea V, Rinne SA, Boppart SA. Phase-resolved magnetomotive OCT for imaging nanomolar concentrations of magnetic nanoparticles in tissues. Opt Express 2008;16:11525–39.

36. Xu C, Vinegoni C, Ralston TS, Luo W, Tan W, Boppart SA. Spectroscopic spectral-domain optical coherence microscopy. Opt Lett 2006;31:1079–81.

37. Lee TM, Oldenburg AL, Sitafalwalla S, et al. Engineered microsphere contrast agents for optical coherence tomography. Opt Lett 2003;28:1546–8.

38. Yang C. Molecular contrast optical coherence tomography: a review. Photochem Photobiol 2005;81:215–37.

39. Zysk AM, Nguyen FT, Oldenburg AL, Marks DL, Boppart SA. Optical coherence tomography: a review of clinical development from bench to bedside. J Biomed Opt 2007;12:051403.

40. Zysk AM, Boppart SA. Computational methods for analysis of human breast tumor tissue in optical coherence tomography images. J Biomed Opt 2006;11:054015.

41. Arifler D, Guillaud M, Carraro A, Malpica A, Follen M, Richards-Kortum R. Light scattering from normal and dysplastic cervical cells at different epithelial depths: finite-difference time-domain modeling with a perfectly matched layer boundary condition. J Biomed Opt 2003; 8:484–94.

42. Drezek R, Guillaud M, Collier T, et al. Light scattering from cervical cells throughout neoplastic progression: influence of nuclear morphology, DNA content, and chromatin texture. J Biomed Opt 2003;8:7–16.

43. Hsiung PL, Phatak DR, Chen Y, Aguirre AD, Fujimoto JG, Connolly JL. Benign and malignant lesions in the human breast depicted with ultrahigh resolution and three-dimensional optical coherence tomography. Radiology 2007;244:865–74.

44. Goldberg BD, Iftimia NV, Bressner JE, et al. Automated algorithm for differentiation of human breast tissue using low coherence interferometry for fine needle aspiration biopsy guidance. J Biomed Opt 2008;13:014014.

45. Zysk AM, Adie SG, Armstrong JJ, et al. Needle-based refractive index measurement using low-coherence interferometry. Opt Lett 2007;32:385–7.

46. Zysk AM, Chaney EJ, Boppart SA. Refractive index of carcinogen-induced rat mammary tumours. Phys Med Biol 2006;51:2165–77.

47. Nguyen FT, Zysk AM, Kotynek JG, et al. Portable real-time optical coherence tomography system for intraoperative imaging and staging of breast cancer. In: Vo-Dinh T, Grundfest WS, Benaron DA, Cohn GE, Raghavachari R, editors. Proceedings of SPIE - Photonics West, Biomedical Optics - Advanced Biomedical and Clinical Diagnostic Systems V. 2007;6430:64300H.

48. Bouma BE, Tearney GJ, Yabushita H, et al. Evaluation of intracoronary stenting by intravascular optical coherence tomography. Heart 2003;89:317–20.

49. Ralston TS, Marks DL, Carney PS, Boppart SA. Interferometric synthetic aperture microscopy. Nat Phys 2007;3:129–34.

50. Abramson RG, Mavi A, Cermik T, et al. Age-related structural and functional changes in the breast: multimodality correlation with digital mammography, computed tomography, magnetic resonance imaging, and positron emission tomography. Semin Nucl Med 2007;37:146–53.